

NEUROSCIENCE

Dual-vector gene therapy restores cochlear amplification and auditory sensitivity in a mouse model of DFNB16 hearing loss

Olga Shubina-Oleinik¹, Carl Nist-Lund¹, Courtney French², Shira Rockowitz², A. Eliot Shearer^{1,2}, Jeffrey R. Holt^{1,3*}

Hearing loss affects an estimated 466 million people worldwide, with a substantial fraction due to genetic causes. Approximately 16% of genetic hearing loss is caused by pathogenic mutations in *STRC*, a gene that encodes the protein stereocilin. To develop gene therapy strategies for patients with *STRC* hearing loss, we generated a mouse model with a targeted deletion in the *Strc* gene. We devised a novel dual-vector approach to circumvent the size limitation of AAV vectors and drive expression of full-length *STRC* protein. To target outer hair cells, which are difficult to transduce, we used synthetic AAV9-PHP.B vectors for efficient dual-vector transduction. We report robust recovery of exogenous *STRC* expression in outer hair cells of *Strc*-deficient mice, recovery of hair bundle morphology, substantially improved cochlear amplification, and enhanced auditory sensitivity. The data raise the prospect that our strategy could benefit ~2.3 million patients worldwide affected by *STRC* mutations.

INTRODUCTION

The mammalian inner ear has evolved a unique ability to amplify soft sounds, attenuate its response to loud sounds, and sharply tune its response in the frequency domain. Collectively, these functions, known as cochlear amplification, depend on the activity of sensory outer hair cells in the cochlea (1). Cochlear amplification requires cohesive outer hair cell bundles and a physical connection between hair bundle tips and the overlying tectorial membrane (2). A key protein required to couple hair bundles to the tectorial membrane and maintain cohesive hair bundles is known as stereocilin (3, 4). With functional stereocilin, the cochlear amplifier can improve auditory thresholds by ~60 dB, thus enhancing sensitivity to faint sounds by a million-fold.

Unfortunately, the gene that encodes human stereocilin (*STRC*) is a common target of genetic mutations that cause recessive hearing loss, known as DFNB16 (5–7). Pathogenic *STRC* mutations include single-nucleotide variants, large genomic rearrangements, gene conversions, and deletions (8). The carrier frequency of *STRC* mutations in the human population has been difficult to determine due to the highly homologous genomic architecture surrounding the *STRC* gene. Although a small study of 152 normal-hearing subjects revealed an *STRC* mutation carrier frequency of 2.6% (9), larger population studies are needed to better understand the contribution of *STRC* mutations to human hearing loss.

Some reports suggest that up to 16% of genetic hearing loss may be due to mutations in *STRC*, making DFNB16 the second most common form of genetic hearing loss and the most common form to affect sensory hair cells (5–8). Patients who carry *STRC* mutations lack cochlear amplification entirely and, as a result, suffer from reduced auditory sensitivity and have difficulty with frequency discrimination and speech perception (10). To address this significant

unmet need, we determined the carrier frequency of *STRC* mutations, generated a mouse model of DFNB16, and designed a dual-vector protein-recombination strategy to replace full-length wild-type (WT) *Strc* in outer hair cells of DFNB16 mice that carry *Strc* mutations.

RESULTS

STRC carrier frequency

The carrier frequency of pathogenic *STRC* mutations in a large cohort of normal-hearing individuals has been difficult to ascertain due to the complexities of DNA sequencing at the highly homologous genomic architecture surrounding the *STRC* gene, 15q15.3 region. Here, we leveraged a large dataset of exome data with integrated phenotypic data from electronic medical records (11) and took an unbiased approach to estimate the number of ethnically mixed normal-hearing children who carry *STRC* mutations. We identified 1256 pediatric subjects with high-quality exome data and without phenotypic evidence of hearing loss. Within this cohort, we identified 22 individuals who carried pathogenic *STRC* mutations, all in the heterozygous state. Sixteen individuals carried full or partial *STRC* deletions, while another six individuals carried pathogenic single-nucleotide variants. Together, these data suggest that the carrier frequency of pathogenic *STRC* mutations is 1.8% in the general normal-hearing population. Extrapolating these data to the U.S. population, we estimate that there are ~107,000 DFNB16 patients with biallelic *STRC* mutations and ~1200 babies born in the United States each year with DFNB16 hearing loss.

Generation of *Strc*-deficient mice

To model DFNB16 hearing loss, we generated mice with a null allele of the *Strc* gene using CRISPR-Cas9 and three single-guide RNAs (sgRNAs) designed to target positions within the fourth exon (Fig. 1A). The coding sequence of the *Strc* gene was disrupted by nonhomologous end joining and yielded a 249–base pair (bp) deletion (Fig. 1B) flanked by two transpositions of inverted sequences. The disruption resulted in a frameshift and premature stop codon that yielded a severely truncated nonfunctional *STRC* protein. To localize stereocilin

Copyright © 2021
The Authors, some
rights reserved;
exclusive licensee
American Association
for the Advancement
of Science. No claim to
original U.S. Government
Works. Distributed
under a Creative
Commons Attribution
NonCommercial
License 4.0 (CC BY-NC).

¹Department of Otolaryngology, Boston Children's Hospital and Harvard Medical School, Boston, MA 02115, USA. ²Children's Rare Disease Cohort Initiative, Boston Children's Hospital, Boston, MA 02115, USA. ³Department of Neurology, Boston Children's Hospital and Harvard Medical School, Boston, MA 02115, USA.

*Corresponding author. Email: jeffrey.holt@childrens.harvard.edu

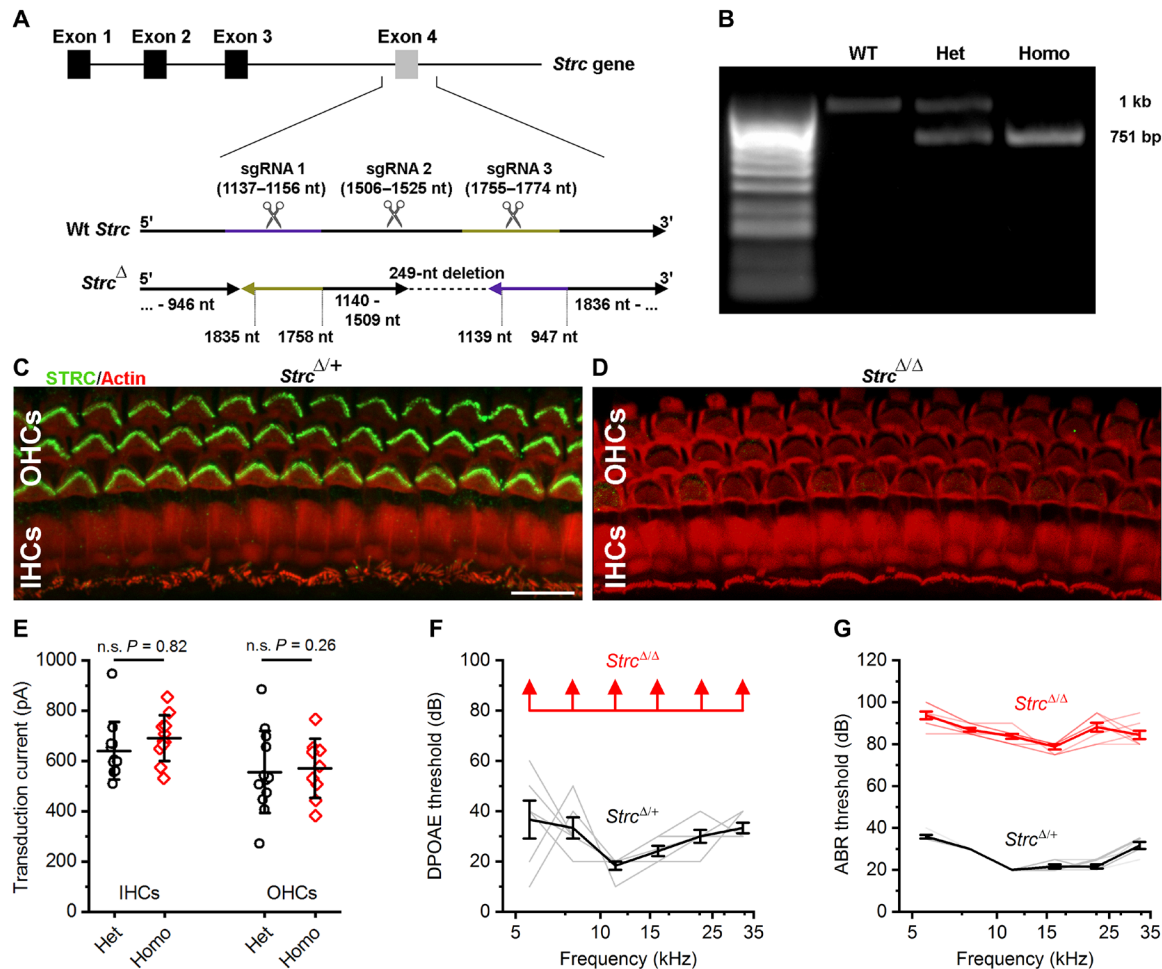


Fig. 1. Generation and characterization of *Strc^{Δ/Δ}* mice. (A) CRISPR-Cas9 strategy for disruption of WT *Strc*. Three single-guide RNAs (sgRNAs) were designed to target exon 4. The gene disruption strategy yielded a 249-nucleotide (nt) deletion and two transpositions and inversions [947–1139 (purple) and 1758–1835 (yellow)], which introduced a premature stop codon in the mutant *Strc* allele. (B) PCR was used to amplify genomic DNA, which, when run on a gel, yielded clear bands for WT (1 kb) and mutant *Strc* (751 bp) alleles. (C and D) Confocal images of *Strc^{Δ/+}* heterozygous and *Strc^{Δ/Δ}* homozygous cochleas taken from tissue stained with an anti-STRC antibody, an Alexa Fluor 488 secondary, and phalloidin–Alexa Fluor 555 to illuminate hair bundles. Inner hair cells (IHCs) and three rows of outer hair cells (OHCs) are indicated. Scale bar, 10 μm. (E) Mean ± SD sensory transduction current amplitudes measured from IHCs and OHCs of *Strc^{Δ/+}* (Het) and *Strc^{Δ/Δ}* (Homo) mice. n.s., not significant. (F) Mean ± SD DPOAE thresholds obtained from *Strc^{Δ/Δ}* mice ($n = 6$; red) and *Strc^{Δ/+}* mice ($n = 6$; black). Data from individual mice shown in light red and gray. (G) Mean ± SD ABR thresholds obtained from *Strc^{Δ/Δ}* mice ($n = 6$; red) and *Strc^{Δ/+}* mice ($n = 6$; black).

and confirm loss of full-length STRC protein in *Strc^{Δ/Δ}* mice, we excised cochleas from postnatal day (P) 30 mice, stained with anti-STRC antibodies and phalloidin to illuminate actin-rich hair bundles. Confocal images revealed robust STRC staining in *Strc^{Δ/+}* heterozygous mouse outer hair cell bundles and lack of STRC staining in inner hair cell bundles. There was no STRC staining in inner or outer hair bundles from *Strc^{Δ/Δ}* mice (Fig. 1, C and D). We evaluated mechano-sensory transduction in inner and outer hair cells from heterozygous controls and homozygous *Strc^{Δ/Δ}* mice at P10. Consistent with a prior report on a similar mouse line (3), we found no significant loss of sensory transduction in inner or outer hair cells, suggesting that various mutations in *Strc* do not disrupt hair cell function or viability (Fig. 1E). However, when we evaluated distortion product otoacoustic emissions (DPOAEs), a measure of cochlear amplification, we found profound loss of function in *Strc^{Δ/Δ}* mice. *Strc^{Δ/Δ}* mice had no measurable DPOAEs even at the loudest sound levels tested,

80 dB (Fig. 1F). We suspect that disruption of STRC uncoupled outer hair cell bundles from the overlying tectorial membrane, preventing cochlear amplification and generation of DPOAEs. As a result, we found that auditory sensitivity was reduced by a million-fold, as indicated by a ~60-dB shift in auditory brainstem response (ABR) thresholds in *Strc^{Δ/Δ}* mice relative to heterozygous control mice (Fig. 1G). We conclude that disruption of the *Strc* gene causes hearing loss due to the lack of cochlear amplification, consistent with the phenotype in human DFNB16 patients (9) and with that of mice bearing a similar mutation in the *Strc* gene (3).

Development of dual-vector strategy

To develop biological treatments for DFNB16 patients, we used our *Strc^{Δ/Δ}* mouse model and designed an adeno-associated virus (AAV)-based gene replacement strategy (12–15). However, because the coding sequence for *Strc* is 5430 bp, too large to fit in a single AAV vector,

we designed a dual-vector approach using intein-mediated protein recombination (16–18). We considered two split sites, selected to avoid predicted structural domains in the STRC protein and to ensure similar-sized fragments for packaging into AAV vectors. Because intein-mediated recombination is facilitated by cysteine residues adjacent to the split (19), we choose a split site for variant 1 between Ser⁷⁴⁶ and Cys⁷⁴⁷ and for variant 2 between Ala⁹⁶⁹ and Cys⁹⁷⁰ (Fig. 2, A and B). The coding sequences for N- and C-terminal inteins were fused to the coding sequences for N- and C-terminal fragments of *Strc*, respectively (Fig. 2A). To facilitate fragment identification, we also fused a Myc tag to the C terminus of the C-terminal fragments for all variants. To evaluate recombination of full-length STRC, dual plasmids encoding variant 1, and separately variant 2, were transfected into human embryonic kidney (HEK) 293 cells. Cell lysates were collected and analyzed by Western blot with anti-Myc antibodies. We observed no evidence of protein recombination using variants 1 and 2. Because the N terminus of the STRC protein includes a signal sequence that may serve to traffic the protein to intracellular compartments (fig. S1), we reasoned that the failure of variants 1 and 2 to recombine may have resulted from the C- and N-terminal fragments being trafficked to different intracellular compartments. To facilitate targeting to the same intracellular compartment and promote recombination of the full-length protein, we fused the signal sequence to the N terminus of the C fragments of variants 1 and 2, upstream of C-intein to generate variants 3 and 4 (Fig. 2A). When dual plasmids encoding variants 3 or 4 were transfected into HEK293 cells, we found that variant 3, containing the signal sequence in both N and C fragments, promoted recombination of full-length STRC protein (Fig. 2C), whereas variant 4 did not (fig. S2).

Dual-vector delivery restores STRC expression

Next, we packaged the coding sequences for N- and C-terminal fragments of variant 3, driven by *Cmv* promoters, into dual AAV9-PHP.B capsids for injection into the inner ears of *Strc*^{Δ/Δ} mice. Mice were injected at P1 with 1 μl of single N- or C-fragment AAVs or 1 μl of a 1:1 dilution of dual N- and C-fragment AAVs. *Strc*^{Δ/Δ} mice injected with dual AAVs revealed prominent STRC localization at the tips of outer hair cell bundles, consistent with the localization pattern in WT outer hair cell bundles and notably different from uninjected *Strc*^{Δ/Δ} bundles (Fig. 3A). In two *Strc*^{Δ/Δ} mice injected with dual AAV vectors, we found that 59% (92 of 156) of outer hair cell bundles had distinct STRC localization. Dual-injected *Strc*^{Δ/Δ} mice also had prominent cell body staining in inner hair cells but no STRC localization to inner hair cell bundles (fig. S3). We did not observe expression of exogenous STRC in other cell types in the cochlea but did note prominent recovery of STRC expression in kinocilia of vestibular hair cell bundles (fig. S4).

Strc^{Δ/Δ} mice injected with 1 μl of single vectors that encoded either N- or C-terminal STRC fragments revealed no STRC protein localization in hair bundles. However, because the anti-STRC antibody recognized an epitope in the C-terminal fragment, we found strong expression of that protein fragment in inner and outer hair cell bodies but not in hair bundles (fig. S5).

To examine the morphology of outer hair cell bundles in greater detail, WT, *Strc*^{Δ/Δ}, and *Strc*^{Δ/Δ} mice injected with dual AAVs cochleas were excised at 4 or 12 weeks of age, processed, and imaged using scanning electron microscopy (SEM). WT cochleas had outer hair cells with well-organized bundles and clearly visible top connectors

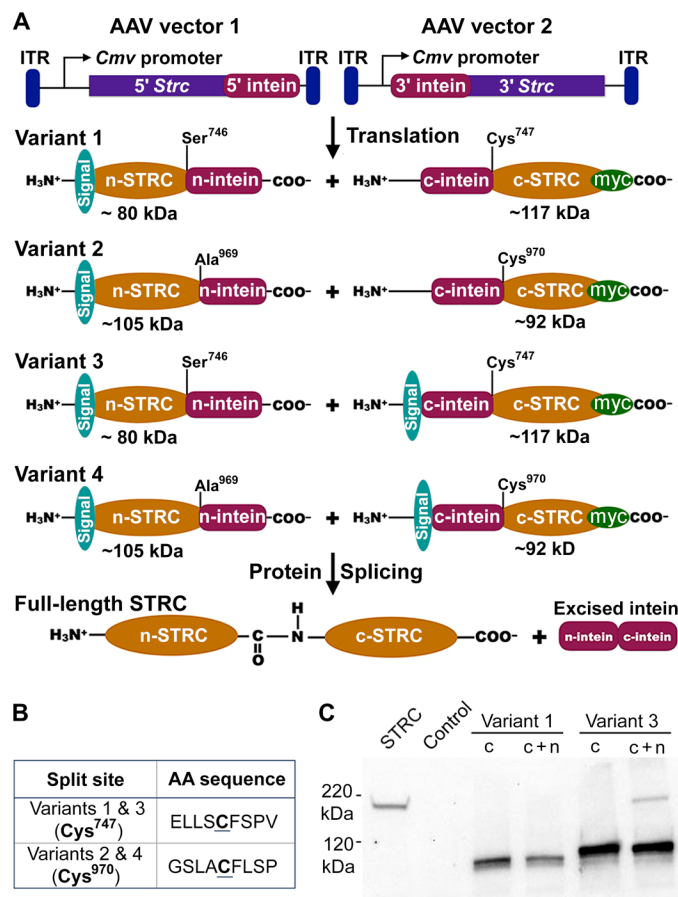


Fig. 2. Dual-vector strategy using intein-mediated protein recombination. (A) Eight AAV2 plasmids were generated that included four dual-vector variant pairs. N- and C-terminal inteins were fused in-frame at the indicated sites for each of the four variants. Variants 1 and 2 differ in their split sites. We took advantage of native cysteines at position 747 (variant 1) and position 970 (variant 2). Variants 3 and 4 had split sites identical to variants 1 and 2, respectively. In addition, variants 3 and 4 had the signal sequence found at the N terminus of STRC fused to the N terminus of the C-terminal fragments, upstream of the C-intein sequence. Inteин-mediated protein recombination was predicted to yield the full-length STRC and an excised intein fragment. A Myc tag was fused to the C terminus of all C-terminal fragments. (B) Split sites and surrounding amino acid sequences for the four variants. (C) Representative Western blot analysis of lysates from HEK293 cells transfected with a plasmid encoding full-length STRC, nontransfected control, plasmids encoding the C-terminal fragments of variants 1 and 3, and cotransfection of both N and C fragments for variants 1 and 3. Anti-Myc antibodies were used to identify C-terminal fragments (120 kDa) and full-length STRC (220 kDa).

linking adjacent stereocilia. *Strc*^{Δ/Δ} cochleas had outer hair cell bundles that lacked top connectors and had mildly but distinctly disorganized hair bundles (Fig. 3B), consistent with loss of contact with the tectorial membrane. SEM images of outer hair cells from *Strc*^{Δ/Δ} mice injected with dual AAVs revealed both normal bundles with top connectors and disorganized bundles lacking top connectors at both 4 and 12 weeks of age. The percentage of bundles with normal organization at 4 weeks was 61% (31 of 51) and was 64% (63 of 99) at 12 weeks. Similarly, we found that the percentage of outer hair bundles in *Strc*^{Δ/Δ} mice injected with dual AAVs with top connectors

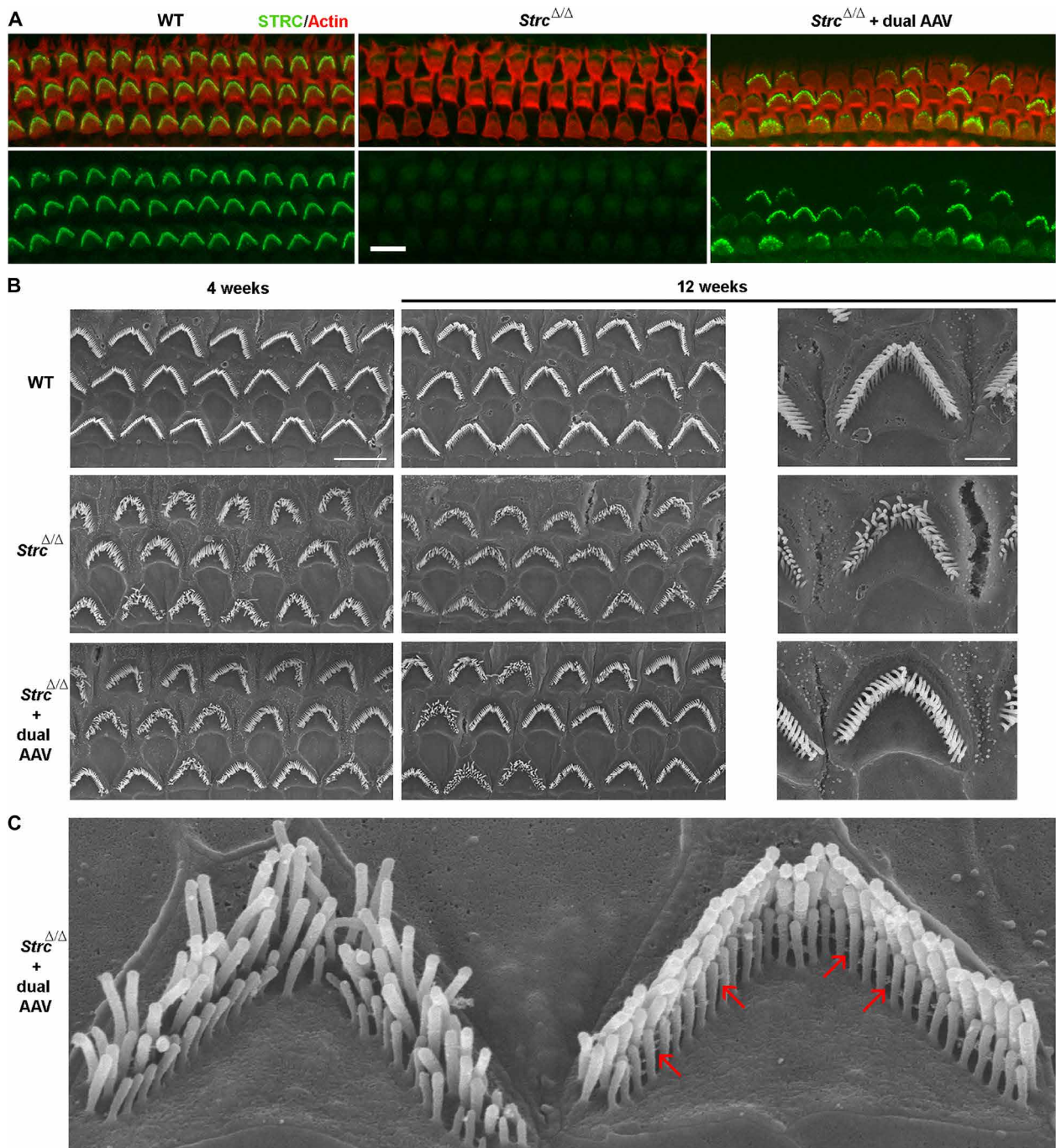


Fig. 3. Dual-AAV delivery restores STRC expression and hair bundle morphology. (A) Confocal images of WT, *Strc*^{Δ/Δ}, and dual vector-injected *Strc*^{Δ/Δ} cochleas stained with an anti-STRC antibody with Alexa Fluor 488-conjugated secondary (green) and Alexa Fluor 555-phalloidin (red). Scale bar, 10 μ m. The top row of images shows that the two channels merged. The bottom row shows STRC localization alone. (B) SEM images of WT, *Strc*^{Δ/Δ}, and dual vector-injected *Strc*^{Δ/Δ} outer hair cell bundles. Tissues were harvested, fixed, and imaged at 4 or 12 weeks as indicated above. Scale bars, 5 μ m (left and middle) or 2 μ m (right). (C) High-magnification view of outer hair bundles from a dual vector-injected *Strc*^{Δ/Δ} cochlea. Red arrows indicate several examples of top connectors between adjacent stereocilia. Note that the bundle to the left lacks top connectors and well-organized stereocilia.

(Fig. 3C) was 65% (37 of 57), consistent with the percentage of outer hair cell bundles that expressed STRC (Fig. 3A). The data suggest that STRC reexpression promotes formation of top connectors and proper hair bundle organization, which together may enable outer hair bundle contact with the tectorial membrane.

Dual-vector delivery restores auditory sensitivity

To determine whether expression of exogenous full-length STRC could restore cochlear amplification, we measured DPOAEs in WT, uninjected *Strc*^{Δ/Δ} mice and *Strc*^{Δ/Δ} mice injected with dual AAVs. The DPOAE assay measures sound emission from the cochlea in

response to two pure tones, referred to as f_1 and f_2 . If active cochlear amplification is present, distortion products are generated at a frequency equal to $2f_1 - f_2$. To analyze sound emission, we performed a Fourier analysis on the emitted waveform and discovered that a $2f_1 - f_2$ distortion product was present in WT mice but absent from $Strc^{\Delta/\Delta}$ mice. The $2f_1 - f_2$ distortion products were present in $Strc^{\Delta/\Delta}$ mice injected with dual AAVs, in some cases with thresholds equivalent to those of WT mice (Fig. 4A). We injected 40 $Strc^{\Delta/\Delta}$ mice with dual AAVs and found successful injections with recovery of DPOAEs in 50% of the mice. DPOAE thresholds were plotted as a function of f_2 frequency and revealed recovery over a broad frequency range from 5.6 to 32 kHz (Fig. 4B). In five mice with the best recovery, DPOAE thresholds averaged 40 dB at 16 kHz. On the basis of the DPOAE assay, the data suggest that dual-vector gene replacement of full-length STRC can restore cochlear amplification in a mouse model of DFNB16. In some mice that lacked DPOAE recovery, we

observed lower expression of STRC, perhaps at a level that was insufficient for functional recovery. This may have been a consequence of poor targeting of injection needles, insufficient dual vector transduction, or inefficient protein recombination.

Given the recovery of DPOAEs in 50% of dual-injected animals, we predicted that auditory sensitivity, as measured by ABR thresholds, would also recover. Analysis of ABR waveforms revealed thresholds as low as 30 dB, similar to WT thresholds, in some $Strc^{\Delta/\Delta}$ mice injected with dual AAVs (Fig. 4C). None of the injected mice that lacked DPOAEs showed recovery of ABR thresholds, underscoring the significance of cochlear amplification for recovery of auditory sensitivity (Fig. 4D). However, all 20 mice with DPOAE recovery also displayed robust recovery of ABR thresholds. In the five $Strc^{\Delta/\Delta}$ mice injected with dual AAVs that had the best recovery, auditory sensitivity was improved by a hundred thousand- to a million-fold, as indicated by ABR thresholds that improved by 50 to

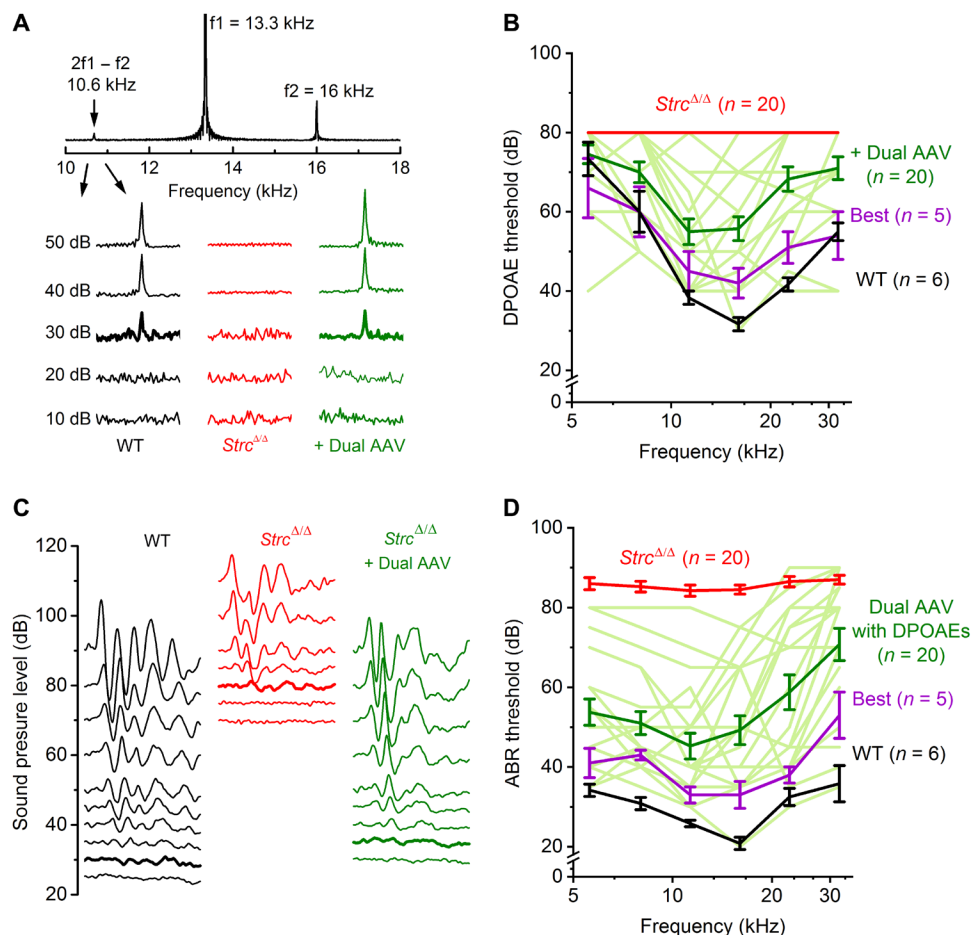


Fig. 4. Dual-AAV delivery restores DPOAE and ABR thresholds 4 weeks after injection. (A) Representative Fourier analysis of DPOAE waveforms revealed two frequency components at the stimulus frequencies f_1 (13.3 kHz) and f_2 (16 kHz) and a distortion product at the predicted frequency $2f_1 - f_2$ (10.6 kHz) in a WT mouse cochlea (top trace). Traces below show the distortion product for sound pressure levels from 10 to 50 dB on an expanded frequency and amplitude scale for WT, $Strc^{\Delta/\Delta}$, and dual vector-injected $Strc^{\Delta/\Delta}$ cochleas. The bold traces indicate the DPOAE threshold. (B) DPOAE thresholds as a function of (f_2) stimulus frequency for WT (black) and dual vector-injected $Strc^{\Delta/\Delta}$ mice with (light green) and without (red) recovery. Red and light green lines represent data from individuals. Mean \pm SE are shown for WT (black), 20 dual vector-injected $Strc^{\Delta/\Delta}$ mice with recovery (green), and the five best recoveries (purple). (C) Families of ABR traces recorded from WT, $Strc^{\Delta/\Delta}$, and dual vector-injected $Strc^{\Delta/\Delta}$ cochleas, evoked by sound pressure levels between 25 and 110 dB. Bold traces indicate ABR thresholds. (D) ABR thresholds plotted as a function of stimulus frequency for WT (black) and dual vector-injected $Strc^{\Delta/\Delta}$ mice with (light green) and without (red) recovery. Light green lines represent data from individuals. Mean \pm SE are shown for WT (black), 20 dual vector-injected $Strc^{\Delta/\Delta}$ mice with (green) and 20 without (red) recovery, and the five $Strc^{\Delta/\Delta}$ mice with the best recoveries (purple).

60 dB (Fig. 4D). The recovery of DPOAE and ABR thresholds persisted out to 12 weeks after injection, the latest time point tested (fig. S6).

Strc^{Δ/Δ} mice injected with single AAVs encoding either N- or C-terminal STRC fragments did not recover DPOAEs, and as a result, there was no recovery of auditory sensitivity. ABR thresholds were indistinguishable from those of uninjected *Strc*^{Δ/Δ} mice (fig. S7). Last, to confirm safety of the dual vector strategy, we injected dual AAV vectors into the inner ears of WT mice and found no change in DPOAE or ABR thresholds (fig. S8), indicating that exogenous expression of STRC fragments, full-length STRC, and the intein proteins were of no consequence for normal auditory function.

DISCUSSION

Here, we provide the largest estimate to date of the carrier frequency for known pathogenic mutations in *STRC*, which cause DFNB16 hearing loss. Using a large database of pediatric subjects without reported hearing loss, we identified a single deletion or known pathogenic single-nucleotide variant in *STRC* in 1.8% of 1256 individuals without hearing loss. This represents the largest assessment of *STRC* mutations within subjects with normal hearing and reinforces prior estimates that homozygous *STRC* mutations are the second most common cause of genetic hearing loss. On the basis of the heterozygous carrier frequency, we estimate that ~2.3 million patients worldwide may carry biallelic pathogenic *STRC* mutations and may be living with DFNB16 hearing loss.

To address this significant unmet need, we generated a new mouse model of DFNB16 that carried a pathogenic deletion in exon 4 of the mouse *Strc* gene. The hearing loss phenotype of our *Strc*^{Δ/Δ} mice is consistent with that of prior reports for *Strc*-deficient mice (3, 4). Verpy *et al.* (3) targeted exons 2 and 3 for excision, whereas our strategy targeted exon 4. Both mouse lines had normal sensory transduction in inner and outer hair cells and demonstrated that DPOAEs were disrupted in the absence of WT *STRC* (3, 4).

To investigate *Strc* gene replacement in our model of DFNB16, we designed an efficient dual-vector strategy for delivery of *STRC* into difficult-to-target outer hair cells of the inner ear using AAV9-PHP.B capsids. To overcome the size limitation of AAV vectors, we devised an intein strategy (16–18) that took advantage of a signal sequence identified at the N terminus of the native *STRC* protein. Intein-mediated recombination has been used for inner ear expression of base editors, where it was found to be efficient in inner hair cells (20). Before this study, intein-mediated recombination has not been used successfully in outer hair cells. By fusing the signal sequence upstream of the C-intein, we reasoned that we could direct both N- and C-protein fragments to the same intracellular compartment to facilitate recombination of full-length *STRC* protein. This general strategy may be useful for gene delivery of other coding sequences too large to be packaged into single AAV vectors. By using either a native signal sequence or the *STRC* signal sequence used here, intein-mediated protein recombination may be an efficient gene replacement strategy for sequences larger than 4.7 kb. Fusion of the signal sequence upstream of the C-intein sequence did not disrupt protein recombination, suggesting that the strategy may be generalizable for other large sequences.

We found that recombination of full-length *STRC* led to recovery of cochlear amplification, a prerequisite for high-sensitivity auditory function, in 50% of injected *Strc*^{Δ/Δ} mice. Although *STRC* dysfunction leads to loss of top connectors, disorganized hair bundle morphologies, and bundles dissociated from the tectorial membrane,

it is important to note that *Strc* mutations did not cause early hair cell death, unlike other hearing loss mutations. If there is a similar lack of hair cell death in humans who harbor *STRC* mutations, we suggest that there may be a broad temporal window for clinical intervention in DFNB16 patients.

Because injection in adult mouse cochleas is technically challenging, we focused on vector delivery during the first postnatal week. Whether dual vector delivery of *STRC* into mature cochleas is a viable treatment option remains to be determined. However, injection into the mature human cochlea may be technically feasible. If it is, given the 1.8% carrier frequency of *STRC* mutations found in this study, we estimate that up to 2.3 million DFNB16 patients worldwide could potentially benefit from *STRC* gene therapy.

MATERIALS AND METHODS

Human genetics

We evaluated patients enrolled as part of a precision medicine initiative called Children’s Rare Disease Cohorts (CRDC), which has previously been described (11). The CRDC leverages exome and genome sequencing from cohorts of pediatric patients with rare diseases. A genomic learning system (GLS) integrates clinical phenotypic data by combing the electronic health record (EHR) and developing pertinent human phenotype ontology (HPO) terms. For this study, we evaluated only unrelated probands (no family members) and excluded patients with HPO terms related to any form of hearing loss using the “hearing impairment” term (HP:0000364) and all of its descendants in the ontology tree.

Exome sequencing was performed at a Clinical Laboratory Improvement Amendments (CLIA)-compliant level from saliva samples (GeneDx, Gaithersburg, MD). Exome-level copy number variant (CNV) calling was performed with GATK (Genome Analysis Toolkit) (21) using a normalized segmented depth of coverage method. To provide validation of this analysis method for CNVs of the 15q15.3 region, a subset of 30 patients with hearing loss was chosen for validation using commercially available multiplex ligation probe amplification (MLPA) regions for the *STRC*-*CATSPER2* region (MRC Holland, Amsterdam, The Netherlands). For these 30 patients, including 4 with homozygous deletions in the region and 2 with hemizygous deletions, there was a 100% concordance rate between exome CNV calls and MLPA. Estimates of numbers of DFNB16 patients were based on the product of the U.S. population (330,000,000), the annual U.S. birth rate (3,750,000), or the world population (7.2 billion) and Hardy-Weinberg equilibrium (heterozygous carrier frequency squared).

Mice

WT C57BL/6J mice (The Jackson Laboratory) were bred on a WT *Cdh23* background, removing the (Ahl) mutation that causes age-related hearing loss. *Strc* mutant mice were generated using the CRISPR-Cas9 system at the Mouse Gene Manipulation Core of the F.M. Kirby Neurobiology Center, Boston Children’s Hospital. In brief, Cas9 mRNA and three sgRNAs [GTTCCCCACAGGGTCCAACG (PAM: CGG), GCTTTACCAAAGGACGACTG (PAM: GGG), and AGGGTG-GCTCTGGGCCTGAG (PAM: TGG)] were microinjected into fertilized embryos of C57BL/6J mice. Mutations in *Strc* gene were confirmed by Sanger sequencing analysis. All procedures met the National Institutes of Health *Guide for the Care and Use of Laboratory Animals* and were approved by the Institutional Animal Care and Use Committees at Boston Children’s Hospital (protocols no. 17-03-3396R

and 18-01-3610R). Mice ages P0 to P1 were used for in vivo delivery of viral vectors according to protocols mentioned above. Male and female mice were randomly chosen for study.

Genotyping

For genotyping, we used the following primers: *Strc* exon 4 forward: GGGTCAAATCTGCAACCGG; *Strc* exon 4 reverse: ACTAAT-TCTGCATTGGCTGC. Polymerase chain reaction (PCR) conditions were as follows: 94°C—3 min [94°C—30 s, 59°C—30 s, 72°C—1 min] × 25, 72°C—5 min, 4°C—thereafter. The PCR products were separated on a 1% agarose gel. The *Strc*^{ΔΔ} allele showed a 751-bp band. The WT allele showed a 1-kb band (Fig. 1B).

Western blot analysis

Samples (HEK293 cells) were lysed in radioimmunoprecipitation assay buffer to extract STRC protein. Lysis buffer was supplemented with protease inhibitors [Halt Protease Inhibitor Cocktail (100×), Thermo Fisher Scientific]. After lysis, samples were denatured at 75°C for 15 min in 1× Laemmli sample buffer. Lysates were separated by 7.5 to 14% SDS–polyacrylamide gel electrophoresis and transferred to hydrophobic polyvinylidene difluoride transfer membrane (Immobilon). An anti-Myc antibody (1:100, [9E1], ChromoTek) was used for immunoblotting to detect the Myc sequence (EQJKUSEEDL) fused to the C terminus of the STRC protein. Horseradish peroxidase-conjugated anti-rat immunoglobulin G (1:1000; GE Healthcare) was used as a secondary antibody. Amersham ECL Prime Western blotting Detection Reagent (GE Healthcare) was used for visualization. Signals were observed, and densitometric analyses were performed on iBright Western blot Imaging Systems (Invitrogen). Each experiment was carried out at least two times.

Tissue preparation

As previously described (15), temporal bones were harvested from mice at 4 or 12 weeks after birth. Mouse temporal bones were harvested after euthanizing the animal with inhaled CO₂, and cochlear half-turns were isolated under a dissection scope via removal of lateral wall tissue and Reissner's membrane with breakable blades (Fine Science Tools) and mechanical removal of tectorial membrane for generation of whole-mount free-floating tissues.

Hair cell electrophysiology

Following established protocols (15), recordings were performed in standard artificial perilymph solution containing 144 mM NaCl, 0.7 mM NaH₂PO₄, 5.8 mM KCl, 1.3 mM CaCl₂, 0.9 mM MgCl₂, 5.6 mM D-glucose, and 10 mM Hepes-NaOH, adjusted to pH 7.4 and 320 mOsmol/kg. Vitamins (1:50) and amino acids (1:100) were added from concentrates (Invitrogen). Hair cells were viewed from the apical surface using an upright Axioskop FS microscope (Zeiss, Oberkochen, Germany) equipped with a 63× water immersion objective with differential interference contrast optics. Recording pipettes (3 to 5 megohms) were pulled from borosilicate capillary glass (Garner Glass) and filled with intracellular solution containing 135 mM KCl, 5 mM EGTA-KOH, 10 mM Hepes, 2.5 mM K₂ATP, 3.5 mM MgCl₂, and 0.1 mM CaCl₂ (pH 7.4). Currents were recorded under whole-cell voltage clamp at a holding potential of −64 mV at room temperature. Data were acquired using an Axopatch 200A (Molecular Devices), filtered at 10 kHz with a low-pass Bessel filter, and digitized at ≥20 kHz with a 12-bit acquisition board (Digidata 1322) and pCLAMP 8.2 and 10.5 (Molecular Devices). Data were analyzed offline with OriginLab software.

Viral vector generation

AAV9-PHP.B viral vectors carrying the coding sequence for the mouse *Strc* gene, inteins, and a cytomegalovirus (*Cmv*) promoter were generated using a helper virus-free system and a double transfection method. AAV9/PHP.B-*Cmv-Strc-n_intein* and AAV9/PHP.B-*Cmv-Strc-c-signal_intein* were produced by the Viral Vector Core at Boston Children's Hospital at titers of 3.1 × 10¹¹ and 1.57 × 10¹¹ genome copies per milliliter, respectively. Titers were calculated by quantitative PCR with hGH (human growth hormone) primers: C-*Strc* forward: GGC-TATTTCTCGATCCCCA, reverse: CAGAGCTGCTTTCTTGTGGG, size: 139 bp and N-*Strc* forward: CCCTGCACTTCGACTTCATG, reverse: CAAGTCCACCCAGTACACCT, size: 158 bp. All vectors were purified using an iodixanol step gradient followed by ion exchange chromatography. Virus aliquots were stored at −80°C and thawed just before use for in vivo injections. Because of the difference in titer, dual AAV9/PHP.B-*Cmv-Strc-n_intein* and AAV9/PHP.B-*Cmv-Strc-c-signal_intein* vectors were mixed at 1:2 ratio by volume to yield a ~1:1 ratio in quantity.

In vivo injections

Utricle injections were performed as approved by the Institutional Animal Care and Use Committees at Boston Children's Hospital (protocol nos. 18-01-3610R and 17-03-3396R). The utricle was identified visually with a stereomicroscope (Zeiss Stemi 2000). One microliter of vector was injected in neonatal WT or *Strc*^{ΔΔ} mice at P1. Mice were anesthetized using hypothermia exposure with ice. Upon anesthesia, post-auricular incision was made to expose the otic bulla and visualize the semicircular canals. Injections were done through the utricle with a glass micropipette filled with AAV vectors as described (22). Standard post-operative care was applied after the injection.

Confocal immunofluorescence

Temporal bones dissected for immunohistochemistry were immersion-fixed for 1 hour at room temperature with 4% paraformaldehyde diluted in phosphate-buffered saline (PBS) after mechanical disruption of the oval and round window membranes and removal of an apical chip for fixative access throughout the cochlea, as previously described (15). After fixation, temporal bones were decalcified in 120 mM EDTA for 24 hours for 4- and 12-week-old tissues before microdissection and isolation of the organ of Corti. The tissues were then rinsed in PBS and permeabilized in 0.02% Triton X-100 for 30 min. Tissues were blocked in 2.5% normal goat serum and 2.5% bovine serum albumin diluted in PBS (blocking solution) for 1 hour and subsequently stained with a rabbit anti-stereocilin primary antibody [produced against synthetic peptide NH₂-970-CFLSPEELQSLVPLSD-COOH derived from the mouse stereocilin amino acid sequence (4); 1:500 dilution in blocking solution; Cocalico Biologicals Inc.] at 4°C overnight. A secondary antibody consisting of a goat anti-rabbit antibody conjugated to Alexa Fluor 488 (1:200 dilution; Life Technologies) and a counterstain to label filamentous actin was applied for 4 to 5 hours. Samples were mounted on glass coverslips with VECTASHIELD mounting medium (Vector Laboratories) and imaged at 63× magnification using a Zeiss LSM 800 confocal microscope. Three-dimensional projection images were generated from Z-stacks using ZEN Blue (ZEISS).

Scanning electron microscopy

Mouse temporal bones were dissected from the surrounding skull base after CO₂ euthanasia. To increase fixative perfusion, holes were made in the round window and oval window membranes along with removal of a small apical piece of bone near the helicotrema. Temporal

bones were placed in 2.5% glutaraldehyde in 0.1 M sodium cacodylate buffer supplemented with 20 mM CaCl₂ for approximately 45 min. Temporal bones were washed in distilled water and then decalcified for approximately 20 hours in 120 mM EDTA (pH 7.4). Temporal bones were washed again with distilled water, and sections of organ of Corti were microdissected out from the surrounding supporting tissue and bone. Tissues were dehydrated in a slowly increasing ethanol series from 50 to 100%. Tissues were transferred to a critical point dryer (Tousimis 931) and mounted on double-sided conductive carbon tape. Tissues were then coated with approximately 4 nm of platinum (Leica ACE600). Images were obtained on a Hitachi S-4700 scanning electron microscope with 5.0-kV accelerating voltage in the Harvard Medical School Imaging and Analysis Core.

Auditory brainstem responses/DPOAE measurement

As previously described (15), ABR recordings were conducted from mice anesthetized via intraperitoneal injection (0.1 ml per 10 g of body weight), with 1 ml of ketamine (50 mg/ml) and 0.75 ml of xylazine (20 mg/ml) diluted into 8.25 ml of 0.9% saline at 4 or 12 weeks of age. ABR experiments were performed at 32°C in a soundproof chamber. To test hearing function, mice were presented pure tone stimuli of 5.6, 8, 11.3, 16, 22.6, or 32 kHz at sound pressure levels between 10 and 90 dB in 5-dB steps until a threshold intensity that evoked a reproducible ABR waveform with an identifiable peak 1 was detected. Acoustic stimuli were delivered directly to the studied ear through a custom probe tube speaker/microphone assembly (EPL PXI Systems) consisting of two electrostatic earphones (CUI miniature dynamics) to generate primary tones and a Knowles miniature microphone (electret condenser) to record ear-canal sound pressure. Sound stimuli consisted of 5-ms tone bursts (0.5-ms rise-fall with a cos² onset, delivered at 40 Hz). ABR signals were collected using subcutaneous needle electrodes inserted at the pinna (active electrode), vertex (reference electrode), and rump (ground electrode). ABR potentials were amplified (10,000×), pass-filtered (0.3 to 10 kHz), and digitized using custom data acquisition software (LabVIEW) from the Eaton-Peabody Laboratories Cochlear Function Test Suite. Sound stimuli and electrode voltage were sampled at 40-μs intervals using a digital I-O board (National Instruments) and stored for offline analysis. Threshold was determined by visual inspection. Data were analyzed and plotted using Origin2015 (OriginLab Corporation, MA).

DPOAE data were collected under the same conditions, and during the same recording sessions, as ABR data. Primary tones were produced at a frequency ratio of 1.2 (f₂/f₁) for the generation of DPOAEs at 2f₁ – f₂, where the f₂ level was 10-dB sound pressure level below f₁ level for each f₂/f₁ pair. The f₂ levels were swept in 10-dB steps from 20 to 80 dB. Waveform and spectral averaging were used at each level to increase the signal-to-noise ratio of the recorded ear-canal sound pressure. The amplitude of the DPOAE at 2f₁ – f₂ was extracted from the averaged spectra, along with the noise floor at nearby points in the spectrum. Iso-response curves were interpolated from plots of DPOAE amplitude versus sound level. Threshold was defined as the f₂ level required to produce DPOAEs above 0 dB.

Statistical analyses

Statistical analyses were performed with Origin 2019 (OriginLab Corporation). Data are presented as mean values ± SD or SE as indicated in the text and figure legends. Error bars and *n* values of biological replicates for experiments are defined in the text and figure legends.

SUPPLEMENTARY MATERIALS

Supplementary material for this article is available at <https://science.org/doi/10.1126/sciadv.abi7629>

[View/request a protocol for this paper from Bio-protocol.](#)

REFERENCES AND NOTES

1. J. Ashmore, Cochlear outer hair cell motility. *Physiol. Rev.* **88**, 173–210 (2008).
2. J. S. Oghalai, The cochlear amplifier: Augmentation of the traveling wave within the inner ear. *Curr. Opin. Otolaryngol. Head Neck Surg.* **12**, 431–438 (2004).
3. E. Verpy, D. Weil, M. Leibovici, R. J. Goodyear, G. Hamard, C. Houdon, G. M. Lefèvre, J.-P. Hardelin, G. P. Richardson, P. Avan, C. Petit, Stereocilin-deficient mice reveal the origin of cochlear waveform distortions. *Nature* **456**, 255–258 (2008).
4. E. Verpy, M. Leibovici, N. Michalski, R. J. Goodyear, C. Houdon, D. Weil, G. P. Richardson, C. Petit, Stereocilin connects outer hair cell stereocilia to one another and to the tectorial membrane. *J. Comp. Neurol.* **519**, 194–210 (2011).
5. L. J. Francey, L. K. Conlin, H. E. Kadesch, D. Clark, D. Berrodin, Y. Sun, J. Glessner, H. Hakonarson, C. Jalas, C. Landau, N. B. Spinner, M. Kenna, M. Sagi, H. L. Rehm, I. D. Krantz, Genome-wide SNP genotyping identifies the stereocilin (STRC) gene as a major contributor to pediatric bilateral sensorineural hearing impairment. *Am. J. Med. Genet. A* **158A**, 298–308 (2012).
6. B. Vona, M. A. H. Hofrichter, C. Neuner, J. Schröder, A. Gehrig, J. B. Hennermann, F. Kraus, W. Shehata-Dieler, E. Klopocki, I. Nanda, T. Haaf, DFNB16 is a frequent cause of congenital hearing impairment: Implementation of STRC mutation analysis in routine diagnostics. *Clin. Genet.* **87**, 49–55 (2015).
7. C. M. Sloan-Heggen, A. O. Bierer, A. E. Shearer, D. L. Kolbe, C. J. Nishimura, K. L. Frees, S. S. Ephraim, S. B. Shibata, K. T. Booth, C. A. Campbell, P. T. Ranum, A. E. Weaver, E. A. Black-Ziegelbein, D. Wang, H. Azaiez, R. J. H. Smith, Comprehensive genetic testing in the clinical evaluation of 1119 patients with hearing loss. *Hum. Genet.* **135**, 441–450 (2016).
8. A. E. Shearer, D. L. Kolbe, H. Azaiez, C. M. Sloan, K. L. Frees, A. E. Weaver, E. T. Clark, C. J. Nishimura, E. A. Black-Ziegelbein, R. J. H. Smith, Copy number variants are a common cause of non-syndromic hearing loss. *Genome Med.* **6**, 37 (2014).
9. Y. Yokota, H. Moteki, S.-Y. Nishio, T. Yamaguchi, K. Wakui, Y. Kobayashi, K. Ohyama, H. Miyazaki, R. Matsuoka, S. Abe, K. Kumakawa, M. Takahashi, H. Sakaguchi, N. Uehara, T. Ishino, T. Koshio, Y. Fukushima, S.-I. Usami, Frequency and clinical features of hearing loss caused by STRC deletions. *Sci. Rep.* **9**, 4408 (2019).
10. A. Simi, J. Perry, E. Schindler, A. Oza, M. Luo, T. Hartman, I. D. Krantz, J. A. Germiller, K. Kawai, M. Kenna, Audiologic phenotype and progression in pediatric STRC-related autosomal recessive hearing loss. *Laryngoscope* **131**, E2897–E2903 (2021).
11. S. Rockowitz, N. LeCompte, M. Carmack, A. Quitadamo, L. Wang, M. Park, D. Knight, E. Sexton, L. Smith, B. Sheidley, M. Field, I. A. Holm, C. A. Brownstein, P. B. Agrawal, S. Kornetsky, A. Poduri, S. B. Snapper, A. H. Beggs, T. W. Yu, D. A. Williams, P. Sliz, Children's Rare Disease Cohorts: An integrative research and clinical genomics initiative. *NPJ Genom. Med.* **5**, 29 (2020).
12. O. Akil, R. P. Seal, K. Burke, C. Wang, A. Alemi, M. Doring, R. H. Edwards, L. R. Lustig, Restoration of hearing in the VGLUT3 knockout mouse using virally mediated gene therapy. *Neuron* **75**, 283–293 (2012).
13. C. Askew, C. Rochat, B. Pan, Y. Asai, H. Ahmed, E. Child, B. L. Schneider, P. Aebischer, J. R. Holt, Tmc gene therapy restores auditory function in deaf mice. *Sci. Transl. Med.* **7**, 295ra108 (2015).
14. D. Dulon, S. Papal, P. Patni, M. Cortese, P. F. Vincent, M. Tertrais, A. Emptoz, A. Tlili, Y. Bouleau, V. Michel, S. Delmaghani, A. Aghaie, E. Pepermans, O. Allegria-Prevot, O. Akil, L. Lustig, P. Avan, S. Safieddine, C. Petit, A. El-Amraoui, Clarin-1 gene transfer rescues auditory synaptopathy in model of Usher syndrome. *J. Clin. Invest.* **128**, 3382–3401 (2018).
15. C. A. Nist-Lund, B. Pan, A. Patterson, Y. Asai, T. Chen, W. Zhou, H. Zhu, S. Romero, J. Resnik, D. B. Polley, G. S. Géléoc, J. R. Holt, Improved TMC1 gene therapy restores hearing and balance in mice with genetic inner ear disorders. *Nat. Commun.* **10**, 236 (2019).
16. K. V. Mills, M. A. Johnson, F. B. Perler, Protein splicing: How inteins escape from precursor proteins. *J. Biol. Chem.* **289**, 14498–14505 (2014).
17. P. Tornabene, I. Trapani, R. Minopoli, M. Centurlo, M. Lupo, S. de Simone, P. Tiberi, F. Dell'Aquila, E. Marrocco, C. Iodice, A. Iuliano, C. Gesualdo, S. Rossi, L. Giaquinto, S. Albert, C. B. Hoyng, E. Polishchuk, F. P. M. Cremers, E. M. Surace, F. Simonelli, M. A. De Matteis, R. Polishchuk, A. Auricchio, Intein-mediated protein trans-splicing expands adeno-associated virus transfer capacity in the retina. *Sci. Transl. Med.* **11**, eaav4523 (2019).
18. J. M. Levy, W.-H. Yeh, N. Pendse, J. R. Davis, E. Hennessey, R. Butcher, L. W. Koblan, J. Comander, Q. Liu, D. R. Liu, Cytosine and adenine base editing of the brain, liver, retina, heart and skeletal muscle of mice via adeno-associated viruses. *Nat. Biomed. Eng.* **4**, 97–110 (2020).

19. N. H. Shah, E. Eryilmaz, D. Cowburn, T. W. Muir, Extein residues play an intimate role in the rate-limiting step of protein trans-splicing. *J. Am. Chem. Soc.* **135**, 5839–5847 (2013).
20. W.-H. Yeh, O. Shubina-Oleinik, J. M. Levy, B. Pan, G. A. Newby, M. Wornow, R. Burt, J. C. Chen, J. R. Holt, D. R. Liu, In vivo base editing restores sensory transduction and transiently improves auditory function in a mouse model of recessive deafness. *Sci. Transl. Med.* **12**, eaay9101 (2020).
21. M. A. DePristo, E. Banks, R. Poplin, K. V. Garimella, J. R. Maguire, C. Hartl, A. A. Philippakis, G. del Angel, M. A. Rivas, M. Hanna, A. McKenna, T. J. Fennell, A. M. Kernysky, A. Y. Sivachenko, K. Cibulskis, S. B. Gabriel, D. Altshuler, M. J. Daly, A framework for variation discovery and genotyping using next-generation DNA sequencing data. *Nat. Genet.* **43**, 491–498 (2011).
22. J. Lee, C. Nist-Lund, P. Solanes, H. Goldberg, J. Wu, B. Pan, B. L. Schneider, J. R. Holt, Efficient viral transduction in mouse inner ear hair cells with utricle injection and AAV9-PHP.B. *Hearing Res* **394**, 107882 (2020).

Acknowledgments: We thank members of the Holt/Géléoc laboratory for helpful feedback and comments on a draft of this manuscript. We also thank B. Pan for assistance with recording hair cell mechanosensory transduction currents. **Funding:** This work was supported by the IDDRC (grant no. 1U54HD090255) including the Neurodevelopmental Behavioral Core, Mouse Gene Manipulation Core, and the Viral Core at Boston Children's Hospital and the

Children's Rare Disease Cohort initiative at Boston Children's Hospital. Gene therapy research in the Holt/Géléoc laboratory is supported by the Jeffrey and Kimberly Barber Fund for Gene Therapy Research, the Usher Syndrome Society, and the Fondation Pour L'Audition.

Author contributions: Conceptualization: O.S.-O. and J.R.H. Methodology: O.S.-O., C.N.-L., C.F., S.R., and A.E.S. Investigation: O.S.-O., C.N.-L., C.F., S.R., and A.E.S. Visualization: O.S.-O. and C.N.-L. Funding acquisition: O.S.-O. and J.R.H. Project administration: J.R.H. Supervision: J.R.H. Writing (original draft): O.S.-O. and J.R.H. Writing (review and editing): All authors.

Competing interests: O.S.-O. and J.R.H. are inventors on a patent for dual-vector delivery of *STRC* for gene therapy in the inner ear. J.R.H. is also an inventor on a patent for use of AAV9-PHP.B for gene delivery to the inner ear. J.R.H. is a scientific founder of Audition Therapeutics and an advisor to several biotech companies focused on inner ear therapeutics. The authors declare no other competing interests. **Data and materials availability:** All data needed to evaluate the conclusions in the paper are present in the paper and/or the Supplementary Materials. The viral plasmids and mice can be provided by J.R.H. pending scientific review and a completed material transfer agreement. Requests for viral plasmids or mice should be submitted to Jeffrey.holt@childrens.harvard.edu.

Submitted 29 March 2021

Accepted 28 October 2021

Published 15 December 2021

10.1126/sciadv.abi7629

Dual-vector gene therapy restores cochlear amplification and auditory sensitivity in a mouse model of DFNB16 hearing loss

Olga Shubina-OleinikCarl Nist-LundCourtney FrenchShira RockowitzA. Eliot ShearerJeffrey R. Holt

Sci. Adv., 7 (51), eabi7629. • DOI: 10.1126/sciadv.abi7629

View the article online

<https://www.science.org/doi/10.1126/sciadv.abi7629>

Permissions

<https://www.science.org/help/reprints-and-permissions>

Use of think article is subject to the [Terms of service](#)

Science Advances (ISSN) is published by the American Association for the Advancement of Science. 1200 New York Avenue NW, Washington, DC 20005. The title *Science Advances* is a registered trademark of AAAS. Copyright © 2021 The Authors, some rights reserved; exclusive licensee American Association for the Advancement of Science. No claim to original U.S. Government Works. Distributed under a Creative Commons Attribution NonCommercial License 4.0 (CC BY-NC).